

SSD-MonoDTR: Supervised Scale-constrained Deformable Transformer for Monocular 3D Object Detection

Xuan He¹ Fan Yang¹ Jiacheng Lin¹ Haolong Fu¹ Jin Yuan^{1,*} Kailun Yang^{2,3} Zhiyong Li^{1,2,3,*}

¹College of Computer Science and Electronic Engineering, Hunan University ²School of Robotics, Hunan University

³National Engineering Research Center of Robot Visual Perception and Control Technology, Hunan University

Abstract

Transformer-based methods have demonstrated superior performance for monocular 3D object detection recently, which predicts 3D attributes from a single 2D image. Most existing transformer-based methods leverage visual and depth representations to explore valuable query points on objects, and the quality of the learned queries has a great impact on detection accuracy. Unfortunately, existing unsupervised attention mechanisms in transformer are prone to generate low-quality query features due to inaccurate receptive fields, especially on hard objects. To tackle this problem, this paper proposes a novel “Supervised Scale-constrained Deformable Attention” (SSDA) for monocular 3D object detection. Specifically, SSDA presets several masks with different scales and utilizes depth and visual features to predict the local feature for each query. Imposing the scale constraint, SSDA could well predict the accurate receptive field of a query to support robust query feature generation. What is more, SSDA is assigned with a Weighted Scale Matching (WSM) loss to supervise scale prediction, which presents more confident results as compared to the unsupervised attention mechanisms. Extensive experiments on “KITTI” demonstrate that SSDA significantly improves the detection accuracy especially on moderate and hard objects, yielding SOTA performance as compared to the existing approaches. Code will be publicly available at [SSD-MonoDETR](#).

1. Introduction

The recent progress in 3D object detection has tremendously promoted its wide applications in autonomous driving [14, 3, 12] and indoor robotics [40, 10]. Benefitting from high-performance hardware, 3D object detection methods based on LiDAR points [53, 37, 48] or binocular images [8, 19, 23] have achieved promising performance, but suffer

*Corresponding author (e-mail: yuanjin@hnu.edu.cn, zhiyong.li@hnu.edu.cn).



Figure 1: Two examples to visualize the predicted key points (circle) on object queries (cross) by (a) MonoDETR and (b) SSD-MonoDTR, where the red indicates the higher attention weight. It is obvious that SSDA could generate key points with higher quality by using the scale-constrained mechanism.

from high hardware costs. Comparatively, monocular 3D object detection [35, 46, 25], which predicts 3D attributes from a single image, could greatly save computation and equipment costs, and thus has attracted more and more research attention.

Most existing monocular 3D detection methods revise the traditional 2D object detectors [22, 34, 42], which either require adjusting abundant manual parameters like anchor, region proposal and NMS [1, 2, 11, 38], or over-depend on exploring the geometric relationship between 2D and 3D objects [18, 44, 41]. Comparatively, newly proposed transform-based detectors like MonoDETR [50]

could avoid tedious parameter settings, and have demonstrated superior performance for monocular 3D object detection [16, 47, 50]. Given an input image with random query points, MonoDETR [50] first adopts several attention operations on visual and depth maps (see Figure 1 (a)) to search for relative key points for each query, and then integrates the features from these key points to predict 3D attributes. Technically, although deformable attention could find the amount of relative key points for a query, still suffers from the serious noisy point problem, especially on hard objects, where many key points deviate to background or irrelative objects (see Figure 1 (a)). This problem stems from the inherent mechanism of deformable attention, which only focuses on exploring relative key points for a query but ignores estimating the receptive field of the query, generating noisy key points outside the object. As a result, the feature aggregation from noisy points would significantly affect 3D attribute prediction.

To alleviate this problem, this paper proposes a Supervised Scale-constrained Deformable Transformer for monocular 3D object detection (SSD-MonoDTR). Different from MonoDTR, SSD-MonoDTR reduces the depth cross-attention layer and introduces a novel Supervised Scale-constrained Deformable Attention (SSDA) layer to emphasize key point prediction for each query (see Figure 1 (b)). Specifically, given a query, SSDA first presets several masks with different scales to extract multi-scale local features for the query from the input visual map, as well as predicts the scale probability distribution of the query from the depth map. On this basis, SSDA then adopts a lightweight adaptive layer to learn the receptive field of the query, which could offer valuable scale information for key point prediction. To better guide SSDA, we design a Weighted Scale Matching (WSM) loss to well balance the relative weights among multiple queries for scale prediction without extra labeling costs. As a result, our SSDA could better predict the receptive field of a query to guide key point generation as compared to deformable attention, and thus alleviates the noisy point problem to generate accurate query features for 3D attribute prediction (see Figure 1 (b)). We conduct extensive experiments on KITTI dataset, and the experimental results demonstrate the effectiveness of SSDA especially on moderate and hard objects, yielding SOTA performance as compared to the existing approaches. The contributions of our work are listed as follows:

1. We propose a Supervised Scale-constrained Deformable Attention (SSDA) to improve the quality of the learned queries in transformer. As compared to deformable attention, SSDA could better predict the receptive field of a query to support accurate key point generation, yielding high-quality query features for 3D attribute prediction.

2. We design a Weighted Scale Matching (WSM) loss on SSDA to directly supervise the scale learning of queries without extra labeling costs, which is more effective as compared the existing unsupervised attention mechanisms in transformer.
3. Experimental results on KITTI dataset demonstrate the leading performance of our approach as compared to the state-of-the-art approaches in moderate and hard subsets. Furthermore, the near real-time inference time indicates the high applicability of our method in the real cases.

2. Related Work

The standard monocular 3D object detection approaches only receive a single image as input to predict 3D attributes for objects, and mostly revise 2D object detectors to implement 3D detection [6, 7, 39]. For instance, M3D-RPN [1] proposes to generate 3D region proposals by a depth-aware convolution. MonoRCNN [38] proposes a geometry-based distance decomposition to factor the object distance into more stable physical and projected 2D heights. GUPNet [27] introduces geometry-guided depth uncertainty to solve the error amplification problem. To further enhance the detection accuracy, recent methods have introduced more effective but complicated geometric priors [31, 45]. RTM3D [20] predicts nine key points of a 3D bounding box to explore the 2D-3D geometric relationship to recover the 3D attributes. Monopair [9] further explores the spatial relationship between pairs of objects to augment the 3D location. MonoJSG [21] utilizes pixel-level geometric constraints to progressively refine the depth estimation. Despite success, these image-based approaches usually suffer from the performance bottleneck limited by the monocular image, and thus researchers have attempted to introduce external resources like depth maps [28, 32, 11, 29] and LiDAR [33, 5, 16] to boost performance, which inevitably brings extra costs on data collection and calculation.

Inspired by the successful applications of transformer in 2D object detection [13, 4, 54], recent researchers have turned to paying increasing attention to transformers for monocular 3D object detection, which could save cumbersome post-processing such as non-maximum suppression (NMS). For instance, MonoDTR [16] introduces Lidar point clouds as auxiliary supervision of its transformer pipeline and utilizes the learned depth features as the input query of a decoder. Without any extra data, DST3D proposes a novel structure [47] combining Swin Transformer [24] with deep layer aggregation [49] to realize 3D object detection. MonoDETR [50] designs a depth-guided decoder, which utilizes a depth cross-attention layer to extract the global depth cues and a deformable attention layer to aggregate local visual features for queries. Thanks to the

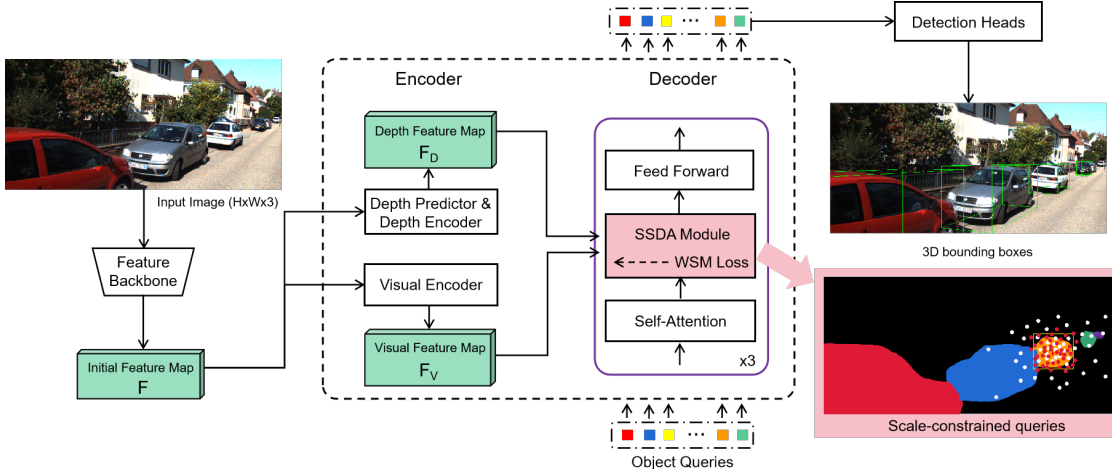


Figure 2: The architecture of SSD-MonoDTR, where SSDA with a WSM loss is introduced to localize the scope of each object query, yielding more accurate query receptive field (the red points) as compared to MonoDETR (the white points).

creative depth-guided decoder, MonoDETR achieves competitive performance.

Differently, this paper focuses on improving the quality of query points in MonoDETR by imposing scale constraints for monocular 3D object detection. We newly design a Supervised Scale-constrained Deformable Attention (SSDA) to replace deformable attention in MonoDETR, which could predict the receptive field of a query to better support accurate feature generation for object queries.

3. Method

3.1. Architecture Overview

Figure 2 demonstrates the architecture of Supervised Scale-constrained Deformable Transformer for monocular 3D object detection (SSD-MonoDTR). Specifically, SSD-MonoDTR first adopts a feature backbone to generate the initial feature map for a given image. On this basis, the visual and depth encoders are employed to extract global visual and depth representations respectively, which are then passed to a transformer decoder to generate valuable queries for object prediction by detection heads. Compared to MonoDETR, SSD-MonoDTR introduces a Supervised Scale-constrained Deformable Attention (SSDA) module to integrate vision and depth information on each object query with a scale constraint, yielding more accurate receptive field as well as better multi-scale local feature representations for object queries. Moreover, we design a Weighted Scale Matching (WSM) loss for SSDA to impose scale constraints on object queries. As a result, our approach could better localize the scope of a query for accurate feature extraction.

3.2. Supervised Scale-constrained Deformable Attention Module

SSDA belongs to the transformer decoder in SSD-MonoDTR and receives the visual embedding \mathbf{F}_V , the depth embedding \mathbf{F}_D , and a set of learnable queries \mathbb{Q} from the last self-attention layer. Specifically, SSDA first extracts multi-scale local visual features for each object query in \mathbb{Q} (see Section 3.2.1), as well as predicts the corresponding depth-guided scale matching probabilities for different scales (see Section 3.2.2). Then, SSDA integrates multi-scale local features and scale matching probabilities by using an adaptively learning layer to form a scale-aware filter, which is used for key point prediction and query updating (see Section 3.2.3).

3.2.1 Query-specific Multi-scale Local Feature Extraction

As Figure 3 shows, given the global visual representation $\mathbf{F}_V \in \mathbb{R}^{\frac{H}{16} \times \frac{W}{16} \times C}$, where H , W , C are the height, width, and channel of an input image, this step aims to generate multi-scale local visual features for each query $q \in \mathbb{Q}$. Here, each query q is initialed with a feature embedding $f_{V,q} \in \mathbb{R}^C$, and a position coordinates (q_x, q_y) . Our approach first takes the query q as the center to generate L masks $\{M_{q,l}\}_{l=1}^L$ with the scale of $l \times l$. Then, the local feature embedding $f_{V,q}^l \in \mathbb{R}^{(l \times l) \times C}$ is generated as follows:

$$f_{V,q}^l = \mathcal{S}_V(\mathbf{F}_V, M_{q,l}), \quad (1)$$

where \mathcal{S}_V is a feature sampler. For the $l \times l$ elements within $M_{q,l}$, \mathcal{S}_V extracts the corresponding feature embedding from \mathbf{F}_V according to their position coordinates. This generates a local visual embedding $f_{V,q}^l$ to capture the vi-

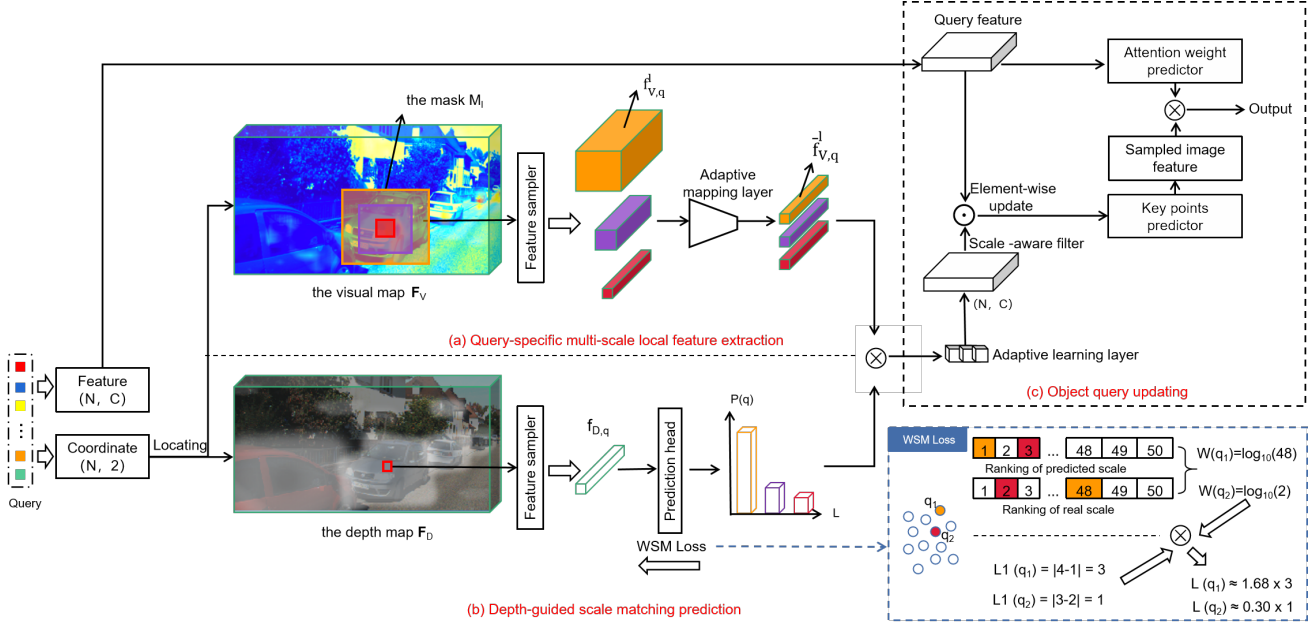


Figure 3: The detailed implementation of SSDA, which is composed of three steps: (a) query-specific multi-scale local feature extraction, (b) depth-guided scale matching prediction, and (c) object query updating.

sual representations for q at the scale of $l \times l$. Finally, we integrate all the local embeddings in $f_{V,q}^l$ to calculate an average local feature $\bar{f}_{V,q}^l \in \mathbb{R}^C$ as follows:

$$\bar{f}_{V,q}^l = \frac{1}{l \times l} \sum_{l \times l} f_{V,q}^l, \quad (2)$$

where $\bar{f}_{V,q}^l$ reflects the average local feature representation at the scale of $l \times l$. For each query q , our approach utilizes L masks to generate L local feature embedding $\{\bar{f}_{V,q}^l\}_{l=1}^L$, which could well capture multi-scale local feature information around q .

3.2.2 Depth-guided Scale Matching Prediction

As Figure 3 shows, given the depth representation $\mathbf{F}_D \in \mathbb{R}^{\frac{H}{16} \times \frac{W}{16} \times C}$, our approach first employs a depth feature sampler \mathcal{S}_D to directly extract the corresponding feature embedding $f_{D,q} \in \mathbb{R}^C$ from \mathbf{F}_D for each query q :

$$f_{D,q} = \mathcal{S}_D(\mathbf{F}_D, q). \quad (3)$$

Intuitively, the depth representation $f_{D,q}$ reflects the object scale of a query to some extent, and thus it is reasonable to design a projection function to map $f_{D,q}$ to a scale matching probability distribution $P(q)$, which is formulated as follows:

$$P(q) = \sigma(f_{D,q}), \quad (4)$$

where σ is a project function implemented by convolution followed by softmax. $P(q)$ is a L -dimensional vector to

represent the L scale matching probabilities, which correspond to the L local feature representations $\{\bar{f}_{V,q}^l\}_{l=1}^L$ in section 3.2.1.

The true scale of q is reflected in the ground truth, and we expect the predicted scale to be consistent with the true value. Thus, we devise a scale matching loss to guide the learning of scale prediction:

$$L(q) = \|P(q, l) * l - \hat{l}_q\|_{L_1}, \quad (5)$$

where $\|\cdot\|_{L_1}$ is L_1 loss, \hat{l}_q is the true scale of q , $P(q, l)$ is the predicted probability on the scale l , and $P(q, l) * l$ represents the predicted scale of q . $L(q)$ reflects the scale prediction error on q , and different queries have different error values during training. To accelerate the model's convergence, it is expected that more attention is paid to the queries with larger errors, and thus we assign a penalty weight item $W(q)$ to $L(q)$ to form our Weighted Scale Matching (WSM) loss, which is expressed as:

$$L_{WSM} = \frac{1}{|\mathbb{B}|} \sum_{q \in \mathbb{B}} W(q)L(q), \quad (6)$$

where \mathbb{B} represents a batch set of queries. $W(q)$ reflects the importance of queries, and we adopt a query ranking mechanism to estimate it. Specifically, for all the queries in \mathbb{B} , our approach generates two query ranking queues Q_P , Q_T in descending order according to their predicted scales and true scales, respectively, and $W(q)$ is calculated as:

$$W(q) = \log(|Index(Q_T, q) - Index(Q_P, q)| + 1), \quad (7)$$

where $Index(Q, q)$ represents the ranking index of q in Q . When q has the same index in both queues, $W(q) = 0$. Otherwise, the large index difference between $Index(Q_T, q)$ and $Index(Q_P, q)$ indicates that the predicted scale has a large error, and thus it is required to give a high penalty weight on q . Compared to the previous loss weighting approaches [17, 36], our ranking mechanism considers the relative weighting correlations among all the queries in a training batch, which is more reasonable and global-aware.

3.2.3 Object Query Updating

Given an initial query, our query updating aims to search for several key points around the query, and then integrate these key points with attention weights to represent the query feature. As aforementioned, although MonoDETR utilizes both depth and visual features to predict key points, there still exist many noise key points. To alleviate this problem, as Figure 3 shows, our query updating utilizes both multi-scale local visual features and scale-matching probability to construct a scale-aware filter to help find more accurate key points. Concretely, given the multi-scale local feature and the scale-matching probability of a query, our approach first multiplies them and then employs an adaptive learning layer to generate a scale-aware filter. Here, the adaptive learning layer contains a lightweight convolutional network with an active layer. Next, we execute the element-wise operation between the filter and the initial query feature to generate the scale-constrained features to better predict key points. Finally, the query feature is updated by integrating these key points features with the attention weights. Benefitting from the scale-aware filter, our approach could predict accurate key points to better support query feature generation for 3D attribute prediction.

3.3. Training Loss

SSD-MonoDTR is an end-to-end network, and all the components are jointly trained according to a composite loss function, which consists of three parts: the 2D object loss L_{2D} to predict object classes, 2D sizes, box IoU, and projected 3D center, the 3D object loss L_{3D} to predict 3D sizes, orientation and depth, and the WSM loss L_{WSM} to estimate the scales of queries. To offer better query features and coordinates, L_{2D} , L_{3D} work on detection heads to ensure the accuracy of object prediction, and L_{WSM} is equipped on SSDA module to improve query features. As a result, our composite loss is expressed as:

$$L = L_{2D} + L_{3D} + \lambda L_{WSM}, \quad (8)$$

where λ is a balancing weight.

4. Experiments

4.1. Experimental Setup

Dataset: We verify SSD-MonoDTR on the popular KITTI 3D object detection benchmark [14], including 7,481 training and 7,518 testing images. Considering the unseen labels on the testing set, we follow [7] to further split the training samples into 3,712 sub-training set and 3,769 validation set. We measure the detection results on three-level difficult samples (easy, moderate, and hard), and evaluate the performance on the class ‘‘Car’’ by using the average precision (AP) in 3D space and the bird-eye view, denoted as AP_{3D} and AP_{BEV} , respectively, which are at 40 recall positions.

Implementation Details: We adopt ResNet-50 [15] as our feature backbone, and follow the settings of MonoDETR except the decoder. We first set the number N of queries as 50. For SSDA, we select 5 scales $\{1, 3, 5, 7, 9\}$ to extract local features, where the channel C of features is 256. There are total 8 heads inside SSDA. To train our model, we follow MonoDETR to set the weights inside L_{2D} and L_{3D} , and the balancing weight λ of L_{WSM} in Equation 8 is 0.2. Our training is conducted on a single RTX A6000 GPU by using Adam optimizer with a weight decay 10^{-4} for 200 epochs, where the batch size is 16 and the learning rate is 2×10^{-4} .

4.2. Performance Comparison

Table 1 demonstrates the performance comparison results of the car category on KITTI test and val sets. We compare our approach with several advanced approaches by using or not using extra data. From the table, we can draw the following conclusions:

1. Among all the approaches, SSD-MonoDTR achieves the best accuracies on moderate and hard objects, with 0.83% – 4.81% improvements. This improvement accelerates as sample difficulty increases, which is consistent with the characteristics of our technology. This is because hard samples usually have small sizes, and thus the estimated query points by the previous algorithms are prone to deviate from objects, resulting in detection errors. Comparatively, SSDA could well estimate the scales of query points by using depth-guided scale matching prediction, bringing a significant performance improvement.
2. We discover that our approach achieves greater performance improvements on AP_{BEV} as compared to AP_{3D} . This is because AP_{BEV} mainly focuses on evaluating the relative positions of cars with respect to streets in bird view, which is highly related to the positions of the estimated query points. Comparatively, AP_{3D} pays more attention to size parameters inside

Method	Reference	Test, AP_{3D}			Test, AP_{BEV}			Val, AP_{3D}			Val, AP_{BEV}			Time (ms)
		Easy	Mod.	Hard	Easy	Mod.	Hard	Easy	Mod.	Hard	Easy	Mod.	Hard	
With extra data:														
PatchNet [28]	ECCV2020	15.68	11.12	10.17	22.97	16.86	14.97	-	-	-	-	-	-	400
D4LCN [11]	CVPR2020	16.65	11.72	9.51	22.51	16.02	12.55	-	-	-	-	-	-	200
MonoRUn [5]	CVPR2021	19.65	12.30	10.58	27.94	17.34	15.24	20.02	14.65	12.61	-	-	-	70
DDMP-3D [43]	CVPR2021	19.71	12.78	9.80	28.08	17.89	13.44	-	-	-	-	-	-	180
CaDDN [33]	CVPR2021	19.17	13.41	11.46	27.94	18.91	17.19	23.57	16.31	13.84	-	-	-	630
AutoShape [26]	ICCV2021	22.47	14.17	11.36	30.66	20.08	15.59	20.09	14.65	12.07	-	-	-	-
MonoDTR [16]	CVPR2022	21.99	15.39	12.73	28.59	20.38	17.14	24.52	18.57	15.51	33.33	25.35	21.68	37
OPA-3D [41]	RAL2023	24.60	17.05	14.25	33.54	22.53	19.22	24.97	19.40	16.59	33.80	25.51	22.13	40
Without extra data:														
MonoDLE [30]	CVPR2021	17.23	12.26	10.29	24.79	18.89	16.00	17.45	13.66	11.68	24.97	19.33	17.01	40
MonoRCNN [38]	ICCV2021	18.36	12.65	10.03	25.48	18.11	14.10	16.61	13.19	10.65	25.29	19.22	15.30	70
MonoGeo [52]	CVPR2021	18.85	13.81	11.52	25.86	18.99	16.19	18.45	14.48	12.87	27.15	21.17	18.35	50
MonoFlex [51]	CVPR2021	19.94	13.89	12.07	28.23	19.75	16.89	23.64	17.51	14.83	-	-	-	30
GUPNet [27]	ICCV2021	20.11	14.20	11.77	-	-	-	22.76	16.46	13.72	31.07	22.94	19.75	-
MonoJSG [21]	CVPR2022	24.69	16.14	13.64	32.59	21.26	18.18	26.40	18.30	15.40	-	-	-	42
MonoDETR [50]	CVPR2022	25.00	16.47	13.58	33.60	22.11	18.60	28.84	20.61	16.38	37.86	26.95	22.80	20
SSD-MonoDTR	-	24.52	17.88	15.69	33.59	24.35	21.98	28.73	21.96	18.50	38.00	29.44	26.94	21
Improvement	vs. Extra ✓	-	0.83	1.44	0.05	1.82	2.76	3.76	2.56	1.91	4.20	3.93	4.81	-
Improvement	vs. Extra ×	-	1.41	2.11	-	2.24	3.38	-	1.35	1.82	0.14	2.49	4.14	-

Table 1: Performance of the car category on KITTI test and val sets, where the first/second best results are highlighted in red/blue fonts, and the improvements are noted in bold fonts.

Multi-scale	Easy	Mod.	Hard
{3, 5, 7}	28.01	20.16	17.03
{3, 5, 7, 9}	29.22	21.67	17.40
{1, 3, 5, 7, 9}	29.53	21.96	18.20
{1, 3, 5, 7, 9, 11}	29.26	20.88	17.55
{1, 3, 5, 7, 9, 11, 13}	27.50	19.79	16.02

Table 2: Performance change by using different scale settings.

objects like the distance assessment from object center to ground, which is less relative to the query points.

- Our approach has a similar testing speed as compared to MonoDETR [50], but achieves better accuracy, especially on moderate and hard objects. Although SSDA brings extra computation costs, our approach reduces a cross-attention operation as compared to Mon-

oDETR, resulting in a similar testing speed.

4.3. Evaluation on SSDA

In this experiment, we first try different scale settings in SSDA to observe the performance trend and then evaluate the quality of the generated query points by SSDA.

Method	Position Precision	Weighted Position Precision
MonoDETR	70.17 %	74.61%
SSD-MonoDTR/WSM	73.56 %	86.13 %
SSD-MonoDTR	76.34%	94.78%

Table 3: The prediction precision of key points by MonoDETR, our method without WSM loss and our complete method.

Multi-scale settings in SSDA: Before SSDA, the input images are resized to 1/16 during feature extraction,

and thus most objects are reduced within 1 to 10 pixels in scale. Therefore, we set the scale value in the range of [1, 13] to observe the performance trend, which is shown in Table 2. Initially, we set three masks in SSDA with the scales {3, 5, 7}, which achieves unsatisfactory performance because many object scales are not covered. Then, we add one more mask with a scale 9, and discover that the performance on easy and moderate objects are significantly improved. On this basis, the further introduction of the scale 1 boosts the performance, especially on hard objects, which usually have small sizes. What is more, the performance begin to degrade as the scales 11 and 13 are added. We guess these scales exceed the sizes of most objects and would interrupt the scale estimation on object queries.

Quality evaluation on query points: We evaluate the quality of query points by the three approaches: MonoDETR, SSD-MonoDTR, and SSD-MonoDTR/WSM (SSD-MonoDTR without using WSM loss), and Table 3 demonstrates the comparison results, which are measured by two quantitative criteria: Position Precision, and Weighted Position Precision. Position precision is equal to the proportion of the number of key points falling inside objects to the total number of all the key points, while weighted position precision additionally multiplies the predicted attention weight of each key point to calculate position precision. Benefitting from SSDA, SSD-MonoDTR could better estimate the scales of key points, and thus achieves better position precision as compared to MonoDETR. Without using WSM loss, SSD-MonoDTR/WSM suffers from a sharp performance drop, which proves the effectiveness of WSM loss in supervising the scale prediction. What is more, we discover that the improvement in weighted position precision is enlarged as compared to position precision, which indicates that SSD-MonoDTR gives large attention weights to key points inside objects.

Figure 4 lists an example to visualize the generated key points by MonoDETR and SSD-MonoDTR. Obviously, as compared to MonoDETR, the distribution of the predicted key points by SSD-MonoDTR is more concentrated on objects with larger weights. As a result, SSD-MonoDTR could better learn query features to support object detection.

4.4. Evaluation of Weighted Scale Matching Loss

In this experiment, we first try different weights λ of Weighted Scale Matching (WSM) loss in Equation 8, and then evaluate the effectiveness of the penalty weight item $W(q)$ in Equation 7.

Table 4 demonstrates the performance trend with respect to different weights. When λ increases from 0 to 0.2, the performance is significantly improved by about 2% on all the samples. This is because the use of WSM loss supervises the scale prediction for query points, and thus could offer better query features for object detection. What

λ	Easy	Mod.	Hard
0	27.53	19.54	16.30
0.1	28.85	20.31	17.14
0.2	29.53	21.96	18.20
0.3	29.06	20.57	17.67
0.4	28.04	19.67	17.03
0.5	26.33	18.91	15.84

Table 4: Performance trend with respect to different values of λ .

is more, the further increase of λ would lead to a performance drop since a too-large weight on WSM loss would overshadow the utility of L_{2D} , L_{3D} detection losses, yielding prediction errors.

To verify the effectiveness of the penalty weight item

Form	Easy	Mod.	Hard
WSM loss-0	28.81	20.68	17.12
WSM loss-L1	29.12	21.05	17.79
WSM loss	29.53	21.96	18.20

Table 5: Performance comparison among the three weighting schemes for WSM loss.

$W(q)$ in Equation 7, we compare our WSM loss with the following two settings: WSM loss-0 without using the weight $W(q)$ by setting $W(q) = 1$, and WSM loss-L1 by setting $W(q) = \log L(q)$ which indicates the weight of a query is proportional to its prediction error. Table 5 shows the performance comparison results. Compared to WSM loss-0, WSM loss-L1 achieves better performance because it assigns larger training weights to error samples. Furthermore, our WSM loss considers the global-aware weighting correlations among all the queries in a training batch and thus could achieve the best performance.

4.5. Qualitative Results

Figure 5 shows four visualized examples with the detection results by MonoDETR and SSD-MonoDTR. We discover that several small and partially blocked cars are missed by MonoDETR because MonoDETR is easy to lose relevant query points for these hard objects. Comparatively, SSD-MonoDTR estimates the scale of an object query to extract relevant local features inside the object and thus could offer robust query features to support accurate detection on hard samples.



Figure 4: An example to illustrate the distribution of the generated key points by MonoDETR and our SSD-MonoDTR.



Figure 5: Four representative examples to visualize the detection results between MonoDETR (left) and SSD-MonoDTR (right), where the red circles indicate the missing objects.

5. Conclusions

We propose SSD-MonoDTR to first introduce Supervised Scale-constrained Deformable Attention (SSDA) for monocular 3D object detection. Different from the existing

transform-based methods, SSDA could estimate the scale of a query to better capture its receptive field to impose the scale constraints on key point prediction, yielding better query features for 3D attribute prediction. What is more, SSDA adopts supervised learning with a WSM loss without

extra labeling costs, which is more effective as compared to the unsupervised attention in transformer. Extensive experiments and analyses on KITTI have demonstrated the effectiveness of our approach. In the future, SSDA may be embedded into more transformer-based 3D object detection backbones.

References

- [1] Garrick Brazil and Xiaoming Liu. M3d-rpn: Monocular 3d region proposal network for object detection. In *Proceedings of the IEEE/CVF International Conference on Computer Vision*, pages 9287–9296, 2019. [1](#), [2](#)
- [2] Garrick Brazil, Gerard Pons-Moll, Xiaoming Liu, and Bernt Schiele. Kinematic 3d object detection in monocular video. In *Computer Vision—ECCV 2020: 16th European Conference, Glasgow, UK, August 23–28, 2020, Proceedings, Part XXIII 16*, pages 135–152. Springer, 2020. [1](#)
- [3] Holger Caesar, Varun Bankiti, Alex H Lang, Sourabh Vora, Venice Erin Liong, Qiang Xu, Anush Krishnan, Yu Pan, Giancarlo Baldan, and Oscar Beijbom. nuscenes: A multi-modal dataset for autonomous driving. In *Proceedings of the IEEE/CVF conference on computer vision and pattern recognition*, pages 11621–11631, 2020. [1](#)
- [4] Nicolas Carion, Francisco Massa, Gabriel Synnaeve, Nicolas Usunier, Alexander Kirillov, and Sergey Zagoruyko. End-to-end object detection with transformers. In *Computer Vision—ECCV 2020: 16th European Conference, Glasgow, UK, August 23–28, 2020, Proceedings, Part I 16*, pages 213–229. Springer, 2020. [2](#)
- [5] Hansheng Chen, Yuyao Huang, Wei Tian, Zhong Gao, and Lu Xiong. Monorun: Monocular 3d object detection by reconstruction and uncertainty propagation. In *Proceedings of the IEEE/CVF Conference on Computer Vision and Pattern Recognition*, pages 10379–10388, 2021. [2](#), [6](#)
- [6] Xiaozhi Chen, Kaustav Kundu, Ziyu Zhang, Huimin Ma, Sanja Fidler, and Raquel Urtasun. Monocular 3d object detection for autonomous driving. In *Proceedings of the IEEE conference on computer vision and pattern recognition*, pages 2147–2156, 2016. [2](#)
- [7] Xiaozhi Chen, Kaustav Kundu, Yukun Zhu, Andrew G Berneshawi, Huimin Ma, Sanja Fidler, and Raquel Urtasun. 3d object proposals for accurate object class detection. *Advances in neural information processing systems*, 28, 2015. [2](#), [5](#)
- [8] Xiaozhi Chen, Kaustav Kundu, Yukun Zhu, Huimin Ma, Sanja Fidler, and Raquel Urtasun. 3d object proposals using stereo imagery for accurate object class detection. *IEEE transactions on pattern analysis and machine intelligence*, 40(5):1259–1272, 2017. [1](#)
- [9] Yongjian Chen, Lei Tai, Kai Sun, and Mingyang Li. Monopair: Monocular 3d object detection using pairwise spatial relationships. In *Proceedings of the IEEE/CVF Conference on Computer Vision and Pattern Recognition*, pages 12093–12102, 2020. [2](#)
- [10] Angela Dai, Angel X Chang, Manolis Savva, Maciej Halber, Thomas Funkhouser, and Matthias Nießner. Scannet: Richly-annotated 3d reconstructions of indoor scenes. In *Proceedings of the IEEE conference on computer vision and pattern recognition*, pages 5828–5839, 2017. [1](#)
- [11] Mingyu Ding, Yuqi Huo, Hongwei Yi, Zhe Wang, Jianping Shi, Zhiwu Lu, and Ping Luo. Learning depth-guided convolutions for monocular 3d object detection. In *Proceedings of the IEEE/CVF Conference on computer vision and pattern recognition workshops*, pages 1000–1001, 2020. [1](#), [2](#), [6](#)
- [12] Scott Ettinger, Shuyang Cheng, Benjamin Caine, Chenxi Liu, Hang Zhao, Sabeek Pradhan, Yuning Chai, Ben Sapp, Charles R Qi, Yin Zhou, et al. Large scale interactive motion forecasting for autonomous driving: The waymo open motion dataset. In *Proceedings of the IEEE/CVF International Conference on Computer Vision*, pages 9710–9719, 2021. [1](#)
- [13] Peng Gao, Minghang Zheng, Xiaogang Wang, Jifeng Dai, and Hongsheng Li. Fast convergence of detr with spatially modulated co-attention. In *Proceedings of the IEEE/CVF international conference on computer vision*, pages 3621–3630, 2021. [2](#)
- [14] Andreas Geiger, Philip Lenz, and Raquel Urtasun. Are we ready for autonomous driving? the kitti vision benchmark suite. In *2012 IEEE conference on computer vision and pattern recognition*, pages 3354–3361. IEEE, 2012. [1](#), [5](#)
- [15] Kaiming He, Xiangyu Zhang, Shaoqing Ren, and Jian Sun. Deep residual learning for image recognition. In *Proceedings of the IEEE conference on computer vision and pattern recognition*, pages 770–778, 2016. [5](#)
- [16] Kuan-Chih Huang, Tsung-Han Wu, Hung-Ting Su, and Winston H Hsu. Monodtr: Monocular 3d object detection with depth-aware transformer. In *Proceedings of the IEEE/CVF Conference on Computer Vision and Pattern Recognition*, pages 4012–4021, 2022. [2](#), [6](#)
- [17] Tengting Huang, Zhe Liu, Xiwu Chen, and Xiang Bai. Epnet: Enhancing point features with image semantics for 3d object detection. In *Computer Vision—ECCV 2020: 16th European Conference, Glasgow, UK, August 23–28, 2020, Proceedings, Part XV 16*, pages 35–52. Springer, 2020. [5](#)
- [18] Jason Ku, Alex D Pon, and Steven L Waslander. Monocular 3d object detection leveraging accurate proposals and shape reconstruction. In *Proceedings of the IEEE/CVF conference on computer vision and pattern recognition*, pages 11867–11876, 2019. [1](#)
- [19] Peiliang Li, Xiaozhi Chen, and Shaojie Shen. Stereo r-cnn based 3d object detection for autonomous driving. In *Proceedings of the IEEE/CVF Conference on Computer Vision and Pattern Recognition*, pages 7644–7652, 2019. [1](#)
- [20] Peixuan Li, Huaici Zhao, Pengfei Liu, and Feidao Cao. Rtm3d: Real-time monocular 3d detection from object keypoints for autonomous driving. In *Computer Vision—ECCV 2020: 16th European Conference, Glasgow, UK, August 23–28, 2020, Proceedings, Part III 16*, pages 644–660. Springer, 2020. [2](#)
- [21] Qing Lian, Peiliang Li, and Xiaozhi Chen. Monojsq: Joint semantic and geometric cost volume for monocular 3d object detection. In *Proceedings of the IEEE/CVF Conference on Computer Vision and Pattern Recognition*, pages 1070–1079, 2022. [2](#), [6](#)

- [22] Tsung-Yi Lin, Priya Goyal, Ross Girshick, Kaiming He, and Piotr Dollár. Focal loss for dense object detection. In *Proceedings of the IEEE international conference on computer vision*, pages 2980–2988, 2017. 1
- [23] Yuxuan Liu, Lujia Wang, and Ming Liu. Yolostereo3d: A step back to 2d for efficient stereo 3d detection. In *2021 IEEE International Conference on Robotics and Automation (ICRA)*, pages 13018–13024. IEEE, 2021. 1
- [24] Ze Liu, Yutong Lin, Yue Cao, Han Hu, Yixuan Wei, Zheng Zhang, Stephen Lin, and Baining Guo. Swin transformer: Hierarchical vision transformer using shifted windows. In *Proceedings of the IEEE/CVF international conference on computer vision*, pages 10012–10022, 2021. 2
- [25] Zechen Liu, Zizhang Wu, and Roland Tóth. Smoke: Single-stage monocular 3d object detection via keypoint estimation. In *Proceedings of the IEEE/CVF Conference on Computer Vision and Pattern Recognition Workshops*, pages 996–997, 2020. 1
- [26] Zongdai Liu, Dingfu Zhou, Feixiang Lu, Jin Fang, and Liangjun Zhang. Autoshape: Real-time shape-aware monocular 3d object detection. In *Proceedings of the IEEE/CVF International Conference on Computer Vision*, pages 15641–15650, 2021. 6
- [27] Yan Lu, Xinzhu Ma, Lei Yang, Tianzhu Zhang, Yating Liu, Qi Chu, Junjie Yan, and Wanli Ouyang. Geometry uncertainty projection network for monocular 3d object detection. In *Proceedings of the IEEE/CVF International Conference on Computer Vision*, pages 3111–3121, 2021. 2, 6
- [28] Xinzhu Ma, Shinan Liu, Zhiyi Xia, Hongwen Zhang, Xingyu Zeng, and Wanli Ouyang. Rethinking pseudo-lidar representation. In *Computer Vision—ECCV 2020: 16th European Conference, Glasgow, UK, August 23–28, 2020, Proceedings, Part XIII 16*, pages 311–327. Springer, 2020. 2, 6
- [29] Xinzhu Ma, Zihui Wang, Haojie Li, Pengbo Zhang, Wanli Ouyang, and Xin Fan. Accurate monocular 3d object detection via color-embedded 3d reconstruction for autonomous driving. In *Proceedings of the IEEE/CVF International Conference on Computer Vision*, pages 6851–6860, 2019. 2
- [30] Xinzhu Ma, Yinmin Zhang, Dan Xu, Dongzhan Zhou, Shuai Yi, Haojie Li, and Wanli Ouyang. Delving into localization errors for monocular 3d object detection. In *Proceedings of the IEEE/CVF Conference on Computer Vision and Pattern Recognition*, pages 4721–4730, 2021. 6
- [31] Arsalan Mousavian, Dragomir Anguelov, John Flynn, and Jana Kosecka. 3d bounding box estimation using deep learning and geometry. In *Proceedings of the IEEE conference on Computer Vision and Pattern Recognition*, pages 7074–7082, 2017. 2
- [32] Dennis Park, Rares Ambrus, Vitor Guizilini, Jie Li, and Adrien Gaidon. Is pseudo-lidar needed for monocular 3d object detection? In *Proceedings of the IEEE/CVF International Conference on Computer Vision*, pages 3142–3152, 2021. 2
- [33] Cody Reading, Ali Harakeh, Julia Chae, and Steven L Waslander. Categorical depth distribution network for monocular 3d object detection. In *Proceedings of the IEEE/CVF Conference on Computer Vision and Pattern Recognition*, pages 8555–8564, 2021. 2, 6
- [34] Shaoqing Ren, Kaiming He, Ross Girshick, and Jian Sun. Faster r-cnn: Towards real-time object detection with region proposal networks. *Advances in neural information processing systems*, 28, 2015. 1
- [35] Thomas Roddick, Alex Kendall, and Roberto Cipolla. Orthographic feature transform for monocular 3d object detection. *arXiv preprint arXiv:1811.08188*, 2018. 1
- [36] Olaf Ronneberger, Philipp Fischer, and Thomas Brox. U-net: Convolutional networks for biomedical image segmentation. In *Medical Image Computing and Computer-Assisted Intervention—MICCAI 2015: 18th International Conference, Munich, Germany, October 5–9, 2015, Proceedings, Part III 18*, pages 234–241. Springer, 2015. 5
- [37] Hualian Sheng, Sijia Cai, Yuan Liu, Bing Deng, Jianqiang Huang, Xian-Sheng Hua, and Min-Jian Zhao. Improving 3d object detection with channel-wise transformer. In *Proceedings of the IEEE/CVF International Conference on Computer Vision*, pages 2743–2752, 2021. 1
- [38] Xuepeng Shi, Qi Ye, Xiaozhi Chen, Chuangrong Chen, Zhixiang Chen, and Tae-Kyun Kim. Geometry-based distance decomposition for monocular 3d object detection. In *Proceedings of the IEEE/CVF International Conference on Computer Vision*, pages 15172–15181, 2021. 1, 2, 6
- [39] Andrea Simonelli, Samuel Rota Buló, Lorenzo Porzi, Manuel López-Antequera, and Peter Kontschieder. Disentangling monocular 3d object detection. In *Proceedings of the IEEE/CVF International Conference on Computer Vision*, pages 1991–1999, 2019. 2
- [40] Shuran Song, Samuel P Lichtenberg, and Jianxiong Xiao. Sun rgb-d: A rgb-d scene understanding benchmark suite. In *Proceedings of the IEEE conference on computer vision and pattern recognition*, pages 567–576, 2015. 1
- [41] Yongzhi Su, Yan Di, Guangyao Zhai, Fabian Manhardt, Jason Rambach, Benjamin Busam, Didier Stricker, and Federico Tombari. Opa-3d: Occlusion-aware pixel-wise aggregation for monocular 3d object detection. *IEEE Robotics and Automation Letters*, 2023. 1, 6
- [42] Zhi Tian, Chunhua Shen, Hao Chen, and Tong He. Fcos: Fully convolutional one-stage object detection. In *Proceedings of the IEEE/CVF international conference on computer vision*, pages 9627–9636, 2019. 1
- [43] Li Wang, Liang Du, Xiaoqing Ye, Yanwei Fu, Guodong Guo, Xiangyang Xue, Jianfeng Feng, and Li Zhang. Depth-conditioned dynamic message propagation for monocular 3d object detection. In *Proceedings of the IEEE/CVF Conference on Computer Vision and Pattern Recognition*, pages 454–463, 2021. 6
- [44] Tai Wang, ZHU Xinge, Jiangmiao Pang, and Dahua Lin. Probabilistic and geometric depth: Detecting objects in perspective. In *Conference on Robot Learning*, pages 1475–1485. PMLR, 2022. 1
- [45] Tai Wang, Xinge Zhu, Jiangmiao Pang, and Dahua Lin. Fcos3d: Fully convolutional one-stage monocular 3d object detection. In *Proceedings of the IEEE/CVF International Conference on Computer Vision*, pages 913–922, 2021. 2
- [46] Xinshuo Weng and Kris Kitani. Monocular 3d object detection with pseudo-lidar point cloud. In *Proceedings of*

the IEEE/CVF International Conference on Computer Vision Workshops, pages 0–0, 2019. [1](#)

- [47] Zhihong Wu, Xin Jiang, Ruidong Xu, Ke Lu, Yuan Zhu, and Mingzhi Wu. Dst3d: Dla-swin transformer for single-stage monocular 3d object detection. In *2022 IEEE Intelligent Vehicles Symposium (IV)*, pages 411–418. IEEE, 2022. [2](#)
- [48] Qiangeng Xu, Yiqi Zhong, and Ulrich Neumann. Behind the curtain: Learning occluded shapes for 3d object detection. In *Proceedings of the AAAI Conference on Artificial Intelligence*, volume 36, pages 2893–2901, 2022. [1](#)
- [49] Fisher Yu, Dequan Wang, Evan Shelhamer, and Trevor Darrell. Deep layer aggregation. In *Proceedings of the IEEE conference on computer vision and pattern recognition*, pages 2403–2412, 2018. [2](#)
- [50] Renrui Zhang, Han Qiu, Tai Wang, Xuanzhuo Xu, Ziyu Guo, Yu Qiao, Peng Gao, and Hongsheng Li. Monodetr: Depth-aware transformer for monocular 3d object detection. *arXiv preprint arXiv:2203.13310*, 2022. [1](#), [2](#), [6](#)
- [51] Yunpeng Zhang, Jiwen Lu, and Jie Zhou. Objects are different: Flexible monocular 3d object detection. In *Proceedings of the IEEE/CVF Conference on Computer Vision and Pattern Recognition*, pages 3289–3298, 2021. [6](#)
- [52] Yinmin Zhang, Xinzhu Ma, Shuai Yi, Jun Hou, Zhihui Wang, Wanli Ouyang, and Dan Xu. Learning geometry-guided depth via projective modeling for monocular 3d object detection. *arXiv preprint arXiv:2107.13931*, 2021. [6](#)
- [53] Yin Zhou and Oncel Tuzel. Voxelnet: End-to-end learning for point cloud based 3d object detection. In *Proceedings of the IEEE conference on computer vision and pattern recognition*, pages 4490–4499, 2018. [1](#)
- [54] Xizhou Zhu, Weijie Su, Lewei Lu, Bin Li, Xiaogang Wang, and Jifeng Dai. Deformable detr: Deformable transformers for end-to-end object detection. *arXiv preprint arXiv:2010.04159*, 2020. [2](#)